Materials Science & Engineering A 674 (2016) 626–633

Contents lists available at ScienceDirect

Materials Science & Engineering A

journal homepage: www.elsevier.com/locate/msea

Interplay between sample size and grain size: Single crystalline vs. ultrafine-grained chromium micropillars

R. Fritz [a], V. Maier-Kiener [b], D. Lutz [a], D. Kiener [a,*]

[a] Department Materials Physics, Montanuniversität Leoben, Leoben, Austria
[b] Department Physical Metallurgy & Materials Testing, Montanuniversität Leoben, Leoben, Austria

ARTICLE INFO

Article history:
Received 14 June 2016
Received in revised form
4 August 2016
Accepted 5 August 2016
Available online 5 August 2016

Keywords:
Micromechanics
Crystal plasticity
Size effect
Bcc
Ultrafine-grained
In-situ SEM

ABSTRACT

To gain insights into the influence of the microstructure on the strengthening behaviour in confined volumes, single crystalline (sxx) and ultrafine-grained (ufg) Cr micropillars were investigated using in-situ scanning electron microscope microcompression tests. Post-compression images of the sxx pillars indicate crystallographic slip, while the ufg pillars reveal a bulk-like deformation behaviour and an emergence of grains from the sample surface. Stress-strain curves of sxx samples show intermittent flow and a scaling behaviour agreeing well with other bcc metals investigated previously. Also for ufg samples a size-dependent strength with a reduced but non-negligible scaling exponent is determined. This latter ufg size effect contributes to an increasing influence of near-surface grains controlling plastic flow with decreasing pillar diameter. While for micron-sized pillars the strength differs between the two microstructures, the two scaling trends converge for sub-micron pillars with diameters close to the grain size, indicative of a transition from boundary-mediated to single crystal plasticity.

1. Introduction

Since technical devices are getting ever smaller, the requirements for materials performances are generally increasing. Experimental setups were developed to investigate confined volumes, and efforts were made to establish small scale testing techniques. Uchic et al. [1] were the first to report a size effect in pillar compression testing of single crystalline (sxx) Ni. It was observed that the yield stress scales inversely with some power to the pillar diameter d. Many subsequent investigations followed on sxx face-centred-cubic (fcc) and body-centred-cubic (bcc) metals, with power law scaling exponents being agreed to be ~0.6 for fcc [2,3], and 0.2–0.6 for bcc metals [3–5], respectively. The reason for this variation in bcc metals is still under debate [6].

Due to the absence of closest packed planes in the bcc crystal structure, deformation is rate limited by the movement of screw dislocations via the kink pair mechanism [7]. Thermal activation helps to move these kink pairs. Thermally activated processes seem to be the direct reason for an increasing power law scaling exponent towards the fcc value. If thermal activation reaches $\sim 0.2 \cdot T_m$, where T_m is the melting temperature of the metal, the critical temperature (T_c) is typically reached [8]. At this point, screw dislocations propagate through the material with the same velocity as edge dislocations and the scaling exponent approaches 0.6 [2–4,9], the common value of fcc metals.

The scaling behaviour of fcc and bcc metals has been studied by several groups in the last few years. Greer et al. [10] investigated the stress-strain behaviour of Au and Mo pillars, and differences in the scaling behaviour were accounted to varying dislocation mechanisms. Schneider et al. [6] tested various bcc metals with different T_c at room temperature (RT). Hereby, the T_c/RT ratio refers to different thermal contributions to the Peierls stress of various metals. The received wide range in scaling exponents of the bcc metals (Nb, Ta, W, Mo) has been explained by the thermally activated component of the yield stress [7]. These findings were confirmed by Maier et al. [11] using advanced nanoindentation (NI) techniques. More recently, compression tests on sxx W and Ta were carried out at elevated temperature by Torrents Abad et al. [12]. They observed increasing strength scaling behaviour with increasing temperature. However, in the present case of polycrystalline pillars, the size effect is not only composed of a thermal stress contribution. It is also dependent of an intrinsic grain size [13–16].

It is well-known that defect-free whiskers reveal theoretical strength values, whereas pillars with defects lead to the investigated size effect [14]. In other words there could be a preparation induced size effect. For millimetre-sized and micron-sized samples, Janssen et al. [17] investigated Al and found a processing induced strength scaling behaviour. Samples used in our investigations are very large compared to a probably affected

* Corresponding author.
E-mail address: daniel.kiener@unileoben.ac.at (D. Kiener).

http://dx.doi.org/10.1016/j.msea.2016.08.015

surface volume (typically ~50 nm, Kiener et al. [18]) and therefore no significant influence of a processing induced size effect is expected. In fact, Jennings et al. [19] compared Cu pillars produced with and without focused ion beam (FIB) milling and found that size effects are independent of FIB damage.

Attempts were made to analyse pillars containing different defect densities. Bei et al. [14] compared dislocation free and pre-strained Mo whiskers. Their findings reveal no size effect for pillars with more than 11% pre-strain. Schneider et al. [15] and El-Awady et al. [16] pre-strained Ni pillars and found a reduction of the scaling exponent with increasing pre-strain. This was related to cell structures that formed during straining and the increase in dislocation density in the cell walls with increasing pre-strain.

In our work, the dislocation density was further increased by deforming Cr to far more than 100% representative strain. High pressure torsion (HPT) was used to form an ultrafine-grained (ufg) microstructure with mostly high angle grain boundaries [20,21]. FIB milled pillars were compressed in-situ in a scanning electron microscope and the occurring size effect and deformation behaviour of ufg samples were compared with sxx samples.

2. Materials and methods

An sxx Cr rod with a purity of 99.999% was obtained from Mateck GmbH (Jülich, Germany) in (100) orientation. Slices of approximately 1 mm thickness were cut with a diamond wire saw and subsequently ground and polished to a lamella, on which non-tapered pillars in the size range between 200 nm to 4 μm and with an aspect ratio of 2.5–3 were milled with a dual-beam SEM-FIB workstation (Zeiss LEO 1540 XP, Oberkochen, Germany) [22].

The polycrystalline Cr with a purity of 99.9% was provided as sheets by Plansee SE (Reutte, Austria). To achieve an ufg microstructure, the as-received sample was cut via electron discharge machining (EDM, Brother HS-3100) to a cylinder with a diameter of 30 mm and a height of 7 mm and was subsequently deformed via HPT [20,21]. Due to the RT brittleness of Cr (the ductile to brittle transition temperature (DBTT) of the recrystallized microstructure is 320–390 °C [23]), the deformation process was performed at 200 °C. The sample was processed at a pressure of 4.2 GPa with a rotational speed of 0.5 rpm. After 50 rotations and an imposed equivalent strain of ~360, a saturated ufg microstructure was reached. Subsequently, a lamella with $3 \cdot 2 \cdot 1$ mm³ was cut by EDM, followed by thinning, polishing and FIB milling in a similar way as the sxx sample. Due to the radial strain gradient in HPT samples [20,21], the lamella was cut from a disk radius of 14 mm.

Vickers hardness measurements were performed on the as-received polycrystalline sample as well as on ufg samples using a Buehler MicroMet 5104 and a load of 500 gf.

The grain size was determined at the same disk radius of 14 mm using back-scattered electron (BSE) images (Fig. 1a) and electron back scattered diffraction (EBSD) grain orientation maps (Fig. 1b) recorded in an SEM (Zeiss LEO 1525, Oberkochen, Germany). Additionally, a thin lamella was prepared from a disk radius of approximately 14 mm to investigate the microstructure via transmission electron microscopy (TEM, Philips CM 12), shown in Fig. 1c. For interpretation, the arrangement of the HPT principal directions with respect to the compression axes of the pillars are included in Fig. 1a, the inverse pole figure colour code map is shown in the bottom left corner of Fig. 1b, and the diffraction pattern of the corresponding TEM image is presented in Fig. 1c, revealing almost no texture but slightly elongated grains.

The pillar compression tests were carried out at RT in-situ in an SEM (Zeiss LEO 982, Oberkochen, Germany). Tests on samples smaller than 1 μm were performed utilizing a Hysitron PI 85 Picoindenter® using a feedback loop of 200 Hz, while pillars in the size range between 1 μm and 4 μm were tested with an UNAT-SEM indenter (Zwick GmbH & Co. KG, Ulm, Germany) with a feedback loop of 64 Hz, as this device offers higher loads [24] required to deform the large and strong ufg pillars. The indenters were equipped with conductive diamond flat punches with diameters of 6 μm and 8 μm, respectively (Synton-MDP AG, Nidau, Switzerland). Displacement-controlled tests were conducted at constant displacement rates that were adapted to the pillar geometry in order to reach a constant nominal strain rate of 10^{-3} s^{-1}, thereby excluding strain rate influences. The stress-strain curves were calculated from recorded force-displacement data using the top pillar area and height from the untapered samples. The specimens were strained to ~20%, and corrections for sink-in [25] and machine stiffness [26] were taken into account. Furthermore, movies were captured from the compression tests with 1 frame per second to analyse the dynamics of the deformation processes, and high resolution SEM images were taken post-compression to relate them to the corresponding stress-strain curves.

To compare pillar compression with macroscopic results, ufg samples with dimensions of $2 \cdot 2 \cdot 3$ mm³ were also cut by EDM from a disk radius of 14 mm. These samples were tested using a universal tensile testing unit (Zwick GmbH & Co. KG, Ulm, Germany) modified with a load reverse tool to a compression device.

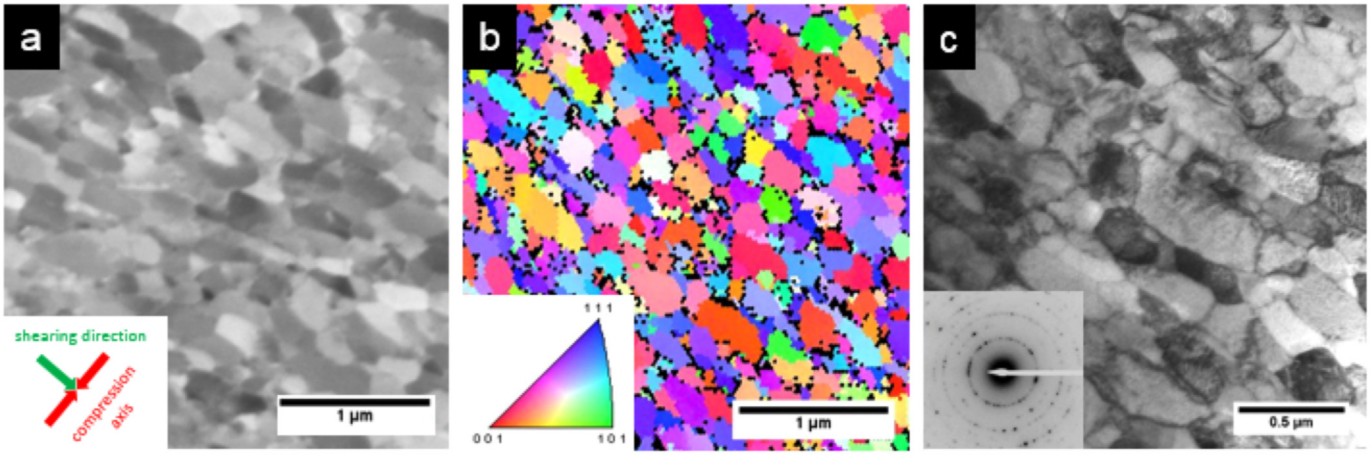

Fig. 1. Microstructure of the HPT deformed Cr. a) BSE image, red arrows in the inset mark the compression axis regarding the direction of shear (green arrow) of the HPT sample, b) EBSD image and corresponding inverse pole figure, and c) bright field TEM image with corresponding diffraction pattern. (For interpretation of the references to color in this figure legend, the reader is referred to the web version of this article.)

Tests were conducted in air at RT and loads were measured with a 10kN load cell. Strains were calculated from the recorded time and corresponding crosshead velocity. The sample was held between two WC-Co plates and sample-plate interface friction was neglected.

3. Results

The bulk hardness of the sxx Cr samples is 1.6 GPa measured by NI [27] and results of Vickers microhardness testing are presented in Table 1. The corresponding indentation sizes for the as-received Cr and the HPT deformed Cr were ~7400 μm^2 and ~2025 μm^2, respectively. The initial grain size of the as-received polycrystalline Cr was ~200 μm. The mean grain sizes of the three images in Fig. 1 were determined at a disk radius of ~14 mm using area-equivalent circle diameters, resulting in average grain sizes of 135 ± 34 nm, 170 ± 84 nm and 150 ± 36 nm for BSE, EBSD and TEM, respectively.

Fig. 2a depicts representative stress-strain curves of the sxx Cr pillars. While small samples show increasing flow stresses, pillar diameters larger than 4 μm reveal a strength of ~600 MPa. Converting the NI hardness (using a constraint factor of 2.8 and $H = \sigma \cdot C^*$ [28]), bulk strengths of ~570 MPa [27] are reached. The data for the bulk yield stress (0.02% plastic strain) of sxx Cr in (100) orientation is reported from tensile tests by Sameljuk et al. [29] as ~290 MPa, a much lower value as observed for present samples. This difference is explained by the large amount of strain hardening between the yield stress and a representative strain of ~8%. For pillars larger than 2 μm, the stress-strain curves show reasonably continuous plastic deformation with occasional burst events, while for smaller samples pronounced load drops occur. At pillar sizes below ~1 μm serrated flow is evident and load drops in the order of 700 MPa are observed. Notably, the number of load drops might also depend on the machine dynamics and whether displacement or load controlled mode is used [30].

In the case of the ufg samples (Fig. 2b), a higher yield stress is reached due to a refined microstructure. NI tests resulted in a strength of ~2050 MPa. Bulk compression samples and pillars with diameters of 4 μm show comparable yield strengths of ~2000 MPa and continuous plastic deformation. However, alignment was hindered due to lower stiffness of the bulk compression equipment, resulting in a sample misalignment of ~1°. Therefore, the elastic loading stiffness of bulk samples is reduced and not comparable with pillar compression experiments, where the determined Young's modulus of 250 GPa is reasonably close to the bulk value of 294 GPa [31].

In the case of decreasing pillar diameter, the yield strength of the ufg pillars also increases slightly. The stress-strain curves show features comparable with those in sxx samples, for instance, serrations and load drops in the order of 300 MPa for the same experimental setting. The plastic deformation behaviour can be seen in the Supplementary videos, where video 1 depicts in-situ SEM pillar compression tests of two ~4 μm sized pillars, sxx and ufg, respectively. The insets show the corresponding stress-strain data. Video 2 depicts the same scheme for pillars with diameters of ~0.6 μm.

Table 1
Purity of the investigated materials and results of hardness testing.

Sample	Purity [%]	Hardness [GPa]
sxx Cr	99.999	1.6 [27]
as-received polycrystalline Cr	99.9	1.2 ± 0.04
ufg Cr	99.9	4.3 ± 0.10

Supplementary material related to this article can be found online at doi:10.1016/j.msea.2016.08.015.

Post-compression SEM images in Fig. 3a and c represent deformed sxx pillars with diameters of ~4 μm and ~0.6 μm. Corresponding stress-strain curves are shown in Fig. 2a where the dark blue curve describes the deformation of the 4 μm sxx pillar and the black curve the deformation of the 0.6 μm sxx pillar, respectively. In case of the large sxx pillar (Fig. 3a), deformation takes place on a preferred slip plane which has been estimated as the (110) plane typical for slip in bcc metals. Due to cross-slip of screw dislocations, deformation occurs on ill-defined crystallographic planes which intersect along the $<111>$ direction [7]. In case of the small sxx pillar shown in Fig. 3c, a similar deformation behaviour governed by crystallographic slip is observed.

Fig. 3b and d represent deformed ufg pillars with diameters of ~3.8 μm and ~0.4 μm. Corresponding stress-strain curves are also depicted in Fig. 2b, where the dark blue curve corresponds to the 3.8 μm ufg pillar and the black curve to the 0.4 μm ufg pillar. In contrast to the sxx samples, the large ufg pillars indicate slight barrelling, which is also seen in macroscopic compression samples due to friction at the surface-tool interfaces. Grains near the free surface emerge and slip planes in the grain interior, corresponding to the planes of highest shear stresses, are visible (Fig. 3d).

In-situ deformation and post-compression SEM images (Fig. 3) reveal the deformation behaviour on the surface, but deformation processes in the pillar volume are not directly visible. Therefore, FIB cross sections of the deformed sxx and ufg pillars were made to perform EBSD scans of the deformed interior. In Fig. 4a, the cross section of a FIB cut sxx pillar is shown with an overlay of the corresponding EBSD scan. The slip traces of the (110) planes are indicated by black lines. The different colours represent a slight rotation of ~2° of the deformed part of the pillar with respect to the base. Fig. 4b and c shows EBSD scans from cross-sections of ufg pillars with diameters of ~4 μm and ~0.5 μm, respectively. Approximately 40,000 grains are located in the volume of the large ufg pillar while the number of grains is reduced to ~80 in the pillar shown in Fig. 4c.

4. Discussion

In general, strengthening occurs when dislocation motion is hindered by obstacles, whether they are precipitates, forest dislocations or grain boundaries [32]. Once the involved length scales are truncated, as in the case of small pillars, the truncation effect is then responsible for the size-dependent strengthening. Moreover, activation of different slip systems can also contribute to a different scaling behaviour [33–36].

To discuss the observed small scale deformation behaviour in detail, the schematic flow stress over pillar diameter diagram and the regarding sample microstructure (Fig. 5a) are considered. As long as Frank-Read sources are controlling plastic deformation, a bulk strength is also expected in miniaturized compression tests, which is schematically represented by the red horizontal line for the sxx case. The obstacle spacing in terms of forest dislocations is smaller than the pillar diameter and a dislocation would bow out between obstacles (depicted as stars) on a preferred slip plane. If the pillar size decreases and the obstacle spacing approaches the pillar diameter, single armed sources [37] are responsible for plastic deformation. This yields to the sample size effect [1–4], evidenced by the increased slope of the red line for the sxx case. The blue lines including the top images in Fig. 5a represent the deformation behaviour of ufg pillars. The top right pillar represents the case of a large sample, where the grain size is noticeably smaller than the pillar size. Dislocations bow out between obstacles or from boundaries in internal grains, and a minority of

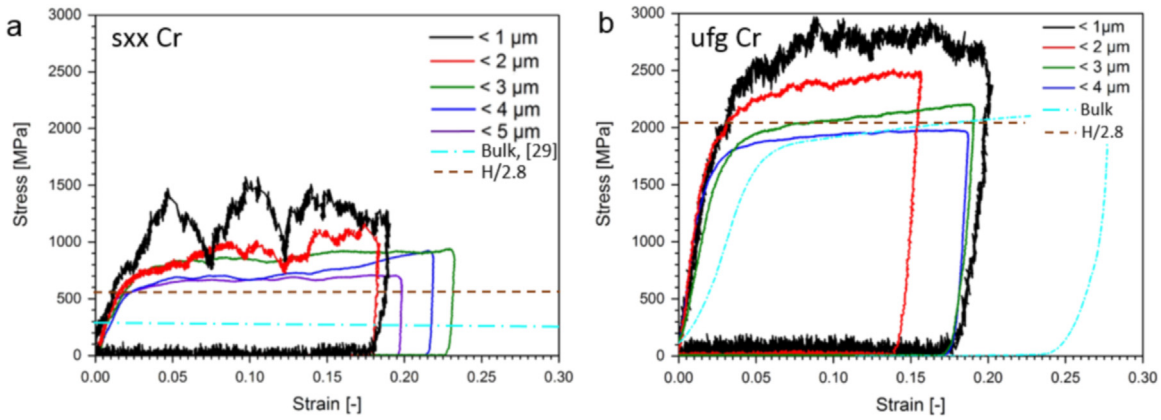

Fig. 2. Representative micro compression stress-strain curves of a) sxx and b) ufg Cr pillars. (For interpretation of the references to color in this figure, the reader is referred to the web version of this article.)

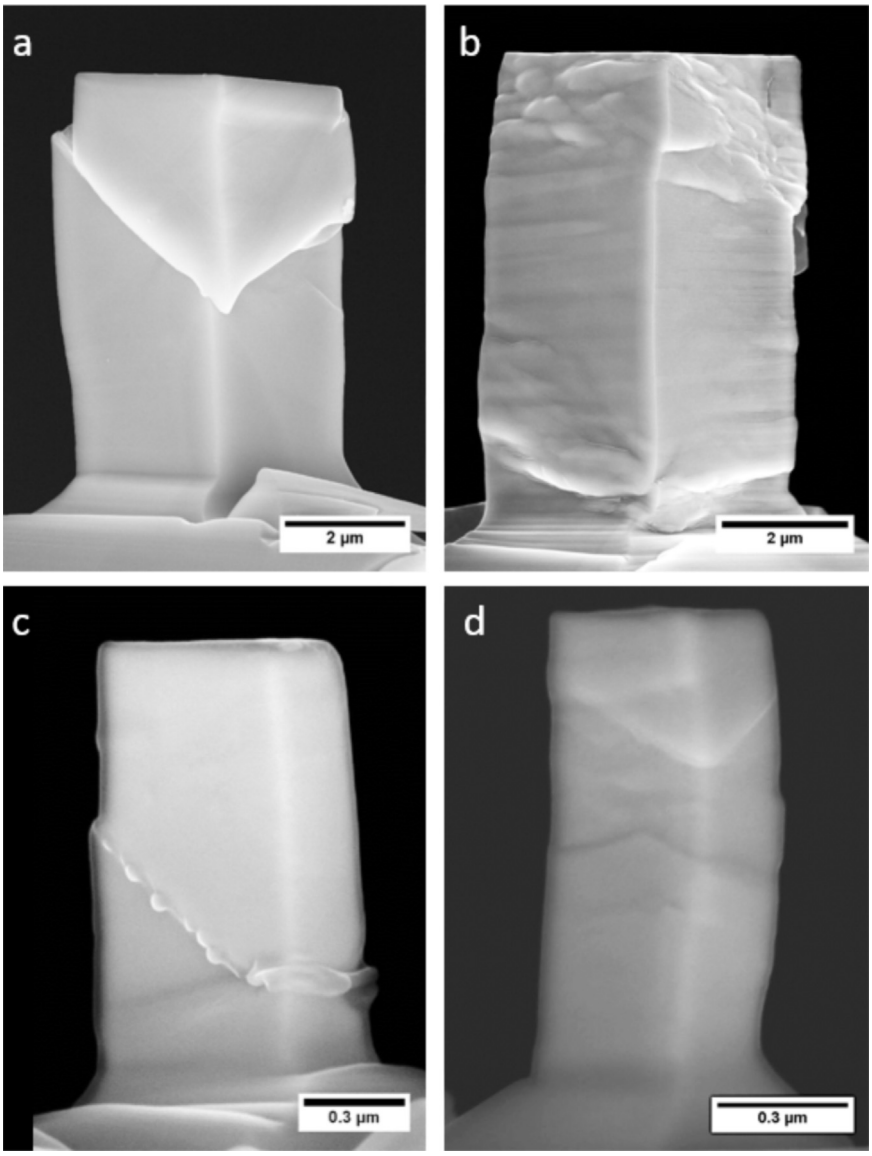

Fig. 3. Post-deformation SEM images of compressed micropillars: a) 4 µm sxx, b) 3.8 µm ufg, c) 0.6 µm sxx and d) 0.4 µm ufg, respectively. All pillars were deformed to ~20% plastic strain.

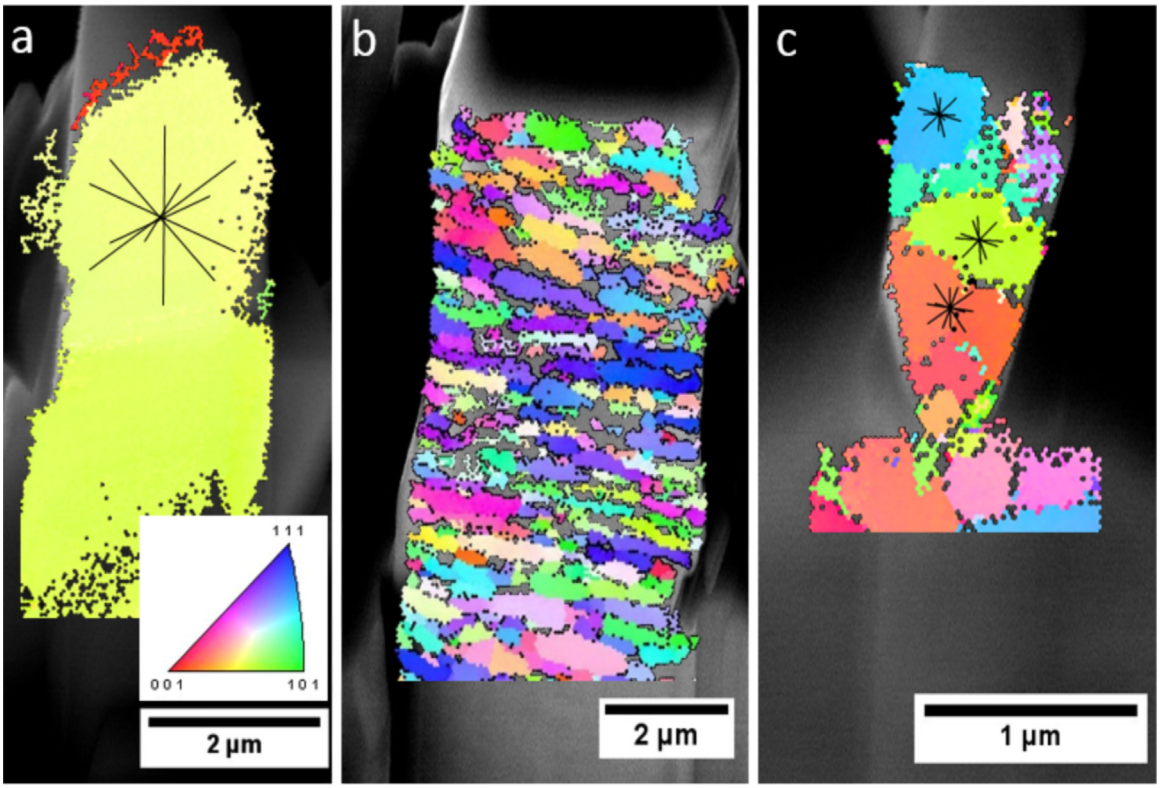

Fig. 4. EBSD scans of cross-sections of different pillars and corresponding inverse pole figure. A) 2 µm sxx Cr pillar with (110) slip trace indicators showing ~2° misorientation between top and bottom part of the pillar, b) a 4 µm ufg pillar, and c) a 0.5 µm ufg pillar with (110) slip trace indicators for the larger grains. (For interpretation of the references to color in this figure, the reader is referred to the web version of this article.)

single armed sources could act in surface grains. The stress-strain behaviour is similar to bulk samples due to a homogenous distribution of grains. The increased polycrystalline strength compared to sxx bulk strength is attributed to Hall-Petch strengthening [38,39]. In this case neither a size effect nor load drops are observable.

If the pillar diameter is decreased for a constant grain size, the number of grains inside the pillar decreases. As a direct consequence less obstacles and pinning points are present in the sample volume. The pillar in the middle of Fig. 5a shows a small ufg specimen where the grain arrangement is not favourable for sxx deformation behaviour, indicated by the marked slip traces of the (110) slip planes that intersect a grain boundary before reaching the pillar surface.

In this simple case, no size effect would be expected, as dislocations are still blocked by grain boundaries, but individual slip events might be detectable in the stress-strain data, as evidenced by load drops in the stress-strain curves for small pillars (Fig. 2). In load-controlled compression tests, strain bursts occur instead of load drops, but their origin is the same [30]. Ufg pillars show such features for pillar diameters smaller than 1 µm, where dislocation avalanches can easily exit at surface grains. Dislocations nucleated in grains being surrounded by other grains cannot exit on free surfaces. They rather pile-up at adjacent grain boundaries, which consequently yields to smaller load drops in the stress-strain curves of larger ufg samples. Such burst events are usually only detected for a limited number of grains. In large samples, they are typically averaged out.

If the grains are oriented in a more favourably way (top left pillar), slip traces reveal no intersections with boundaries and deformation as known for sxx pillars can occur, with the consequence that a size effect will be observed. In a more realistic scenario, surface grains will require higher external loads to cause yielding due to a reduced pile-up contribution for source activation, which will be more important for decreasing pillar diameters. Thus, the transition from ufg to sxx scaling behaviour might be gradual.

Fig. 5b depicts the representative flow stresses of the varying sized Cr pillars, evaluated at 8% plastic strain. This strain value was chosen to allow comparison with hardness tests performed with a Berkovich indenter (imposing 8% plastic strain [28]). Another reason for comparison of stresses at higher strain levels is to include the strain hardening behaviour within the first few percent of deformation to be comparable with previous bcc studies [4,15,33,34]. Red circles and blue squares indicate strength values of sxx and ufg pillars, respectively, with corresponding error bars resulting from uncertainties of determining the cross-sections and the noise of the indenter load without contact as a worst case limit. Horizontal lines on the right represent bulk strengths and were taken for sxx samples from [27]. Bulk strengths of the ufg samples were calculated from hardness testing. They are in good agreement with the macroscopic compression test (Fig. 2b) after removing the error in strain from misalignment.

The slope of the linear fit from the data points of the log-log plot in Fig. 5b gives the power law scaling exponent n, which is 0.43 ± 0.03 for sxx pillars. While the scaling behaviour of bcc sxx pillars is well investigated, Cr has not been examined so far. Thus, it is interesting to note that this value fits well into the concept of Schneider et al. [4]. In fact, if the power law exponent is plotted against the homologous critical temperature (~0.68 for Cr), the model of Schneider would predict a power law scaling exponent of ~0.41, in close agreement with our results.

In the case of ufg pillars, the slope decreases due to the presence of grain boundaries and higher dislocation densities from HPT processing. The linear fit gives a scaling exponent of 0.10 ± 0.02, which reveals that a slight scaling behaviour is evident

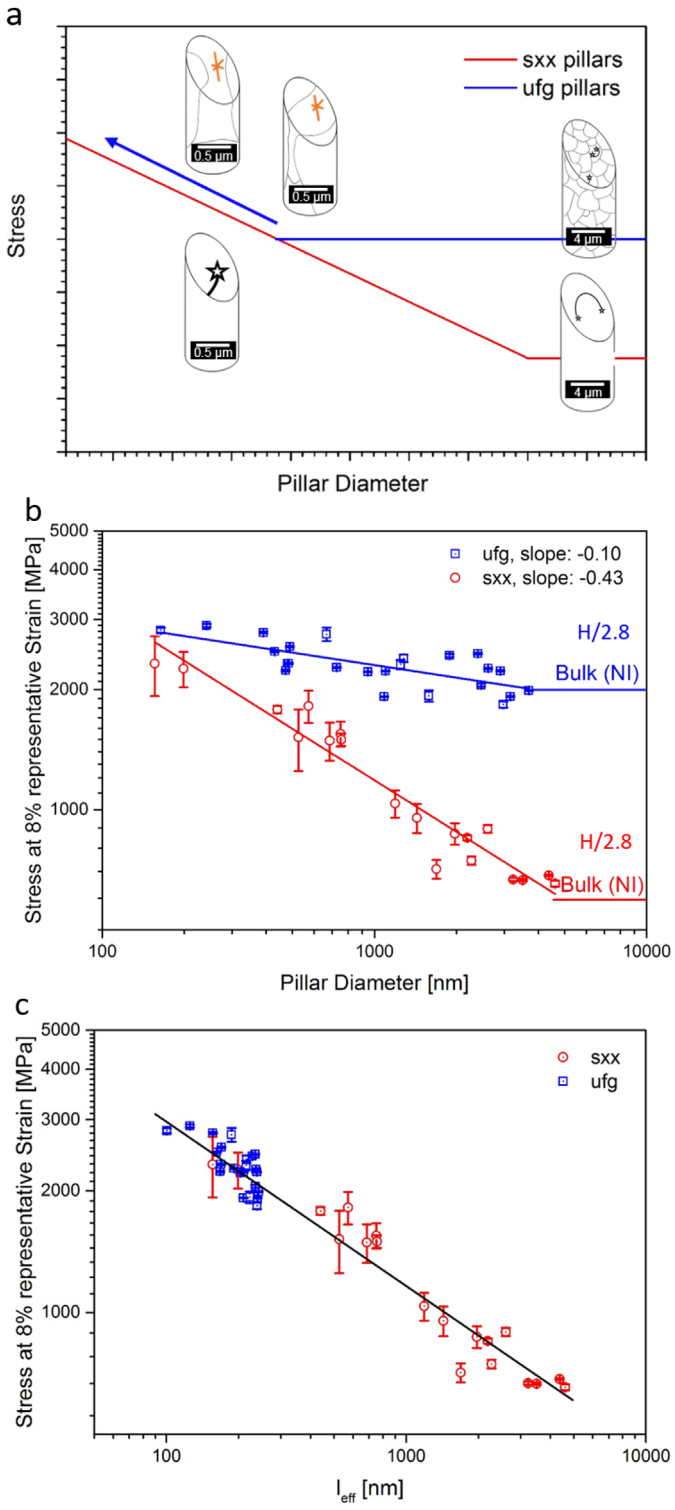

Fig. 5. a) Schematic of the size effect in sxx and ufg pillars in a log-log stress-pillar diameter plot. The red and blue lines represent the behaviour of sxx samples and ufg pillars, respectively. b) Strengthening of sxx Cr and ufg Cr pillars evaluated at 8% flow stress and, c) strength data of both data sets collapses using a combined internal length scale l_{eff}. See text for more details. (For interpretation with reference to colour in the figure legend, the reader is referred to the web version of the article).

even in ufg pillars. The point of intersection of the two fit lines indicates the transition to sxx behaviour. It occurs at a pillar size of ~150 nm, which is in good agreement with the grain size of the material (Fig. 1). In this situation, typically a single grain would span the pillar cross-section, leading to sxx deformation for both material conditions.

From the SEM images in Fig. 3 it appears that the deformation behaviour is different between sxx and ufg pillars, which might have contributed to grain boundary mediated deformation, as reported in [40]. To investigate whether another length scale or deformation mechanism plays a dominant role, both data sets were analysed regarding to dislocation based plasticity. Taking into account sample size as well as grain size in a weakest link concept, many approaches are found in literature. Keller et al. [41] and Chen

et al. [42] investigated the influences of varying sample thickness and grain size on the mechanical properties in tensile tests, while Misra et al. [43], Zhang et al. [44], Guo et al. [45] and Knorr et al. [46] investigated the deformation behaviour in nano-scaled multilayers. Furthermore, Nicola et al. [47] applied such approaches on thin films. Bushby et al. [48] related an indentation contact size with the grain size. First weakest link concepts were suggested by Dunstan et al. [49]. They performed torsion tests on thin wires and related the responsible length scales, the grain size and a structure size (wire diameter) to an effective length scale l_{eff}. For our experiments, the extrinsic pillar diameter D and the intrinsic grain diameter d were related to l_{eff}. The two length scales interact with each other and result in a single scaling effect, for a situation where only dislocation slip is considered:

$$\frac{1}{l_{eff}} = \frac{1}{d} + \frac{1}{D}. \quad (1)$$

The length scale governing plastic deformation in Eq. (1) indicates that the grain size is the dominating part in ufg pillars, whereas for sxx pillars the pillar diameter is dominant (Fig. 5c). For intermediate sizes, the coupling becomes more important. Note that a representative flow stress at 8% strain was again used to scale with the effective length scale of the pillars. It can be seen that sxx and ufg samples collapse on the same trend line (black), which implies that the scaling behaviour in both, ufg and sxx pillars, is controlled by the same deformation mechanism, namely dislocation motion.

The EBSD data, shown in Fig. 4, support these assumptions. The ongoing dislocation motion in the sxx case (Fig. 4a) leads to a slight rotation during compression, which is common behaviour due to lateral constraints [50–52]. Micron-sized ufg pillars (Fig. 4b) deform similarly to bulk samples and show a comparable stress-strain behaviour. Grain size determinations also indicate comparable size distributions as for the initial HPT deformed material mentioned (Fig. 1), and exclude distinct deformation induced grain growth [53,54]. Moreover, no indication of grain boundary sliding is observed in both micron- and sub-micron-sized pillars. In the case of a sub-micron sized pillar (Fig. 4c), sxx deformation behaviour could be expected if one grain would span the whole pillar. For the given grain orientations, slip traces indicate that the grain arrangement is unfavourable for sxx deformation. Therefore, the pillar deforms comparably to the larger ufg pillar with homogeneously distributed grains but at an increased flow stress level compared to bulk, as seen in Fig. 2b.

In the case of polycrystalline pillars, only few and somewhat controversial results are reported in literature. Jang and Greer [55] investigated Ni-W pillars with a grain size of ~60 nm and found a size-induced weakening effect instead of a stress increase with decreasing pillar diameter below ~200 nm. In contrast, Rinaldi et al. [56] investigated comparable pure nanocrystalline Ni with a grain size of about 30 nm for samples in the size range from 160 nm to 272 nm and reported a size effect where smaller pillars are stronger. A scaling exponent of 0.38-0.66 [56] was observed depending on the strain level, where the defect density was always the same. Increasing the dislocation density by pre-straining of sxx Ni reduced the scaling behaviour from 0.66 to 0.16 [15,16].

Schreijäg et al. [57] investigated bcc metals (α-Fe and DC04, a low alloyed steel) with focus on the effect of sample size and microstructure on the strengthening behaviour tested by pillar compression. Their metal sheets were cold rolled and annealed, and the FIB fabricated pillars were in the size range between 500 nm and 22 μm for a grain size of about 50 μm, thus essentially single crystalline. Slip in their heat treated pillars did not necessarily end at grain boundaries and only small differences between sxx and heat treated polycrystalline pillars were found. In the case of the cold rolled material, grain boundaries acting as obstacles were reported not to play an effective role and dislocations did not pile up. Cold rolling resulted in a varying grain boundary character compared to HPT, caused by a much lower degree of deformation. Notably, the contained dislocation density in the rolled material should be comparable with the present ufg material processed via HPT of $\sim 10^{14}$ to 10^{15} m^{-2} [58,59] containing mostly large angle grain boundaries. For Fe, which has a low thermal stress component at RT, the scaling exponent was reported as 0.81 by Schreijäg et al. [57] which is even higher than observed in fcc metals [1,2]. This strong scaling exponent has also been reported by Rogne and Thaulow for sxx Fe [36] and might be contributed to different crystal orientations. A scaling behaviour in strength of the cold rolled DC04 steel has not been observed by Schreijäg *et al*. [57], which is likely due to high dislocation density and large samples, comparable with results of pre-strained pillars [14–16].

Another approach to explain this strengthening is a statistical size effect as suggested by Henning and Vehoff [60]. By calculating Taylor factors and minimal grain areas over the specimen width, they could predict the initial point of yielding in their samples. This, however, requires simplifications such as a two-dimensional microstructure, which is not been guaranteed even in the smallest ufg pillars. Thus, we consider only flow stresses instead of critical resolved shear stresses, and do not attempt to address a statistical size effect.

Jang and Greer [55] and Rinaldi et al. [56] performed their experiments at low grain size to pillar size ratios of ~0.02 to 0.2 corresponding to a bulk situation, while the investigations from Schreijäg et al. [57] were conducted on high d/D ratios of ~2 to 100, thus essentially in the sxx regime. In the case of the present ufg pillars, a grain size to pillar size ratio of ~0.04 to 1 was investigated, thereby spanning the whole range of interest.

In this intermediate transition regime, the results presented show a non-negligible strength scaling behaviour in ufg pillars, emerging due to the comparable magnitude of the internal (microstructural) length scale and the pillar dimensions. Since the grain size d is ~160 nm (Fig. 1), dislocation-mediated plasticity within the grains is most probably responsible for plastic deformation. As dislocations can exit to the surface, stronger near-surface grains gain importance with decreasing sample dimensions. This reduces dislocation pile-ups and local stresses and requires higher loads for plastic deformation. Thereby, near-surface grains contribute to the strength scaling exponent of 0.10 ± 0.02. Considering the situation from the sxx point of view, the reduced scaling exponent would also indicate a higher defect density compared to sxx samples [15]. The defect densities in the investigated samples were not determined explicitly. However, comparison with calculations from El-Awady [61] suggest that a dislocation density of $\sim 10^{14}$ to 10^{15} m^{-2} [58,59] would yield to a scaling exponent of ~0.10, in good agreement with present results.

5. Conclusion

Size effect investigations on sxx Cr and ufg Cr were performed to study the interaction between internal microstructure and external sample dimensions. Sxx pillars reveal a scaling behaviour of ~0.43, in agreement with other bcc sxx pillars when normalized to the homologous critical temperature. Ufg pillars show a decreased scaling behaviour with a scaling exponent of ~0.10. This reduction is explained by the influence of free surfaces in small scale testing, as grains influenced by the pillar surface seem to be stronger than grains in the pillar volume. Dislocations can exit the near-surface grain, making them resistant to subsequent

deformation. Current data analysis is based on dislocation plasticity at RT. Up to now, no differentiation between the effects of dislocation density and grain boundaries regarding the reduced scaling exponent are made. Possible influences of surface or boundary mediated processes, in particular at elevated temperature, will be investigated in the future.

Acknowledgements

The authors want to thank DI Peter Kutleša for help during sample preparation with the HPT device, Gabi Felber for preparation of the thinned lamellas and Plansee SE for providing the bulk material. Financial support by the Austrian Federal Government represented by the Austrian Science Fund FWF (project number: P25325-N20) is gratefully acknowledged. Further financial support by the Austrian Federal Government (837900) (in particular from the Bundesministerium für Verkehr, Innovation und Technologie and the Bundesministerium für Wirtschaft, Familie und Jugend) represented by Österreichische Forschungsförderungsgesellschaft mbH and the Styrian and the Tyrolean Provincial Government, represented by Steirische Wirtschaftförderungsgesellschaft mbH and Standortagentur Tirol, within the framework of the COMET Funding Programme (MPPE, A7.19) is appreciated.

References

[1] M.D. Uchic, D.M. Dimiduk, J.N. Florando, W.D. Nix, Science 305 (2004) 986–989.
[2] M.D. Uchic, P.A. Shade, D.M. Dimiduk, Annu. Rev. Mater. Res. 39 (2009) 8.1–8.26.
[3] J.R. Greer, J.T.M. De Hosson, Prog. Mater. Sci. 56 (2011) 654–724.
[4] A.S. Schneider, D. Kaufmann, B.G. Clark, C.P. Frick, P.A. Gruber, R. Mönig, O. Kraft, E. Arzt, Phys. Rev. Lett. 103 (2009) 105501.
[5] J.-Y. Kim, D. Jang, J.R. Greer, Acta Mater. 58 (2010) 2355–2363.
[6] J. Cui, G. Po, N. Ghoniem, Acta Mater. 108 (2016) 128–137.
[7] B. Sestak, A. Seeger, Z. Metall. 69 (1978) 195–202.
[8] A. Seeger, Z. Metall. 72 (1981) 369–380.
[9] A.S. Schneider, C.P. Frick, E. Arzt, W.J. Clegg, S. Korte, Philos. Mag. Letl. 93 (2013) 331–338.
[10] J.R. Greer, C. Weinberger, W. Cai, Mater. Sci. Eng. A 493 (2008) 21–25.
[11] V. Maier, C. Schunk, M. Göken, K. Durst, Philos. Mag. 95 (2015) 1766–1779.
[12] O. Torrents Abad, J.M. Wheeler, J. Michler, A.S. Schneider, E. Arzt, Acta Mater. 103 (2016) 483–494.
[13] A. Rinaldi, P. Peralta, K. Sieradzki, E. Traversa, S. Licoccia, J. Nanomech. Micromech. 2 (2012) 42–48.
[14] H. Bei, S. Shim, G.M. Pharr, E.P. George, Acta Mater. 56 (2008) 4762–4770.
[15] A.S. Schneider, D. Kiener, C.M. Yakacki, H.J. Maier, P.A. Gruber, N. Tamura, M. Kunz, A.M. Minor, C.P. Frick, Mater. Sci. Eng. A 559 (2013) 147–158.
[16] J.A. El-Awady, M.D. Uchic, P.A. Shade, S.-L. Kim, S.I. Rao, D.M. Dimiduk, C. Woodward, Scr. Mater. 68 (2013) 207–210.
[17] P.J.M. Janssen, J.P.M. Hoefnagels, T.H. de Keijser, M.G.D. Geers, J. Mech. Phys. Solids 56 (2008) 2687–2706.
[18] D. Kiener, C. Motz, M. Rester, M. Jenko, G. Dehm, Mater. Sci. Eng. A 459 (2007) 262–272.
[19] A.T. Jennings, M.J. Burek, J.R. Greer, Phys. Rev. Lett. 104 (2010) 135503.
[20] R. Pippan, S. Scheriau, A. Taylor, M. Hafok, A. Hohenwarter, A. Bachmaier, Annu. Rev. Mater. Res. 40 (2010) 319–343.
[21] R.Z. Valiev, R.K. Islamgaliev, I.V. Alexandrov, Prog. Mater. Sci. 45 (2000) 103–189.
[22] S. Wurster, R. Treml, R. Fritz, M.W. Kapp, E.-M. Langs, M. Alfreider, C. Ruhs, P. J. Imrich, G. Felber, D. Kiener, Prakt. Met. Sonderband 46 (2014) 27–36.
[23] R. Wadsack, R. Pippan, B. Schedler, Fusion Eng. Des. 66–68 (2003) 265–269.
[24] D. Kiener, C. Motz, G. Dehm, R. Pippan, Int. J. Mater. Res 100 (2009) 1074–1087.
[25] I.N. Sneddon, Int. J. Eng. Sci. 3 (1965) 47–57.
[26] D. Kiener, W. Grosinger, G. Dehm, Scr. Mater. 60 (2009) 148–151.
[27] V. Maier, A. Hohenwarter, R. Pippan, D. Kiener, Scr. Mater. 106 (2015) 42–45.
[28] A.G. Atkins, D. Tabor, J. Mech. Phys. Solids 13 (1965) 149–164.
[29] A.V. Sameljuk, A.D. Vasilev, S.A. Firstov, Int. J. Refract. Met. Hard Mater. 14 (1996) 249–255.
[30] O.L. Warren, S.A. Downs, T.J. Wyrobek, Z. Metall. 95 (2004) 287–296.
[31] D.I. Bolef, J. De Klerk, Phys. Rev. 129 (1963) 1063–1067.
[32] E. Arzt, Acta Mater. 46 (1998) 5611–5626.
[33] A.S. Schneider, B.G. Clark, C.P. Frick, P.A. Gruber, E. Arzt, Mater. Sci. Eng. A 508 (2009) 241–246.
[34] A.S. Schneider, C.P. Frick, B.G. Clark, P.A. Gruber, E. Arzt, Mater. Sci. Eng. A 528 (2011) 1540–1547.
[35] S. Korte, W.J. Clegg, Philos. Mag. 91 (2011) 1150–1162.
[36] B.R.S. Rogne, C. Thaulow, Mater. Sci. Eng. A 621 (2015) 133–142.
[37] T.A. Parthasarathy, S.I. Rao, D.M. Dimiduk, M.D. Uchic, D.R. Trinkle, Scr. Mater. 56 (2007) 313–316.
[38] E.O. Hall, Proc. Phys. Soc. Lond. B 64 (1951) 747–753.
[39] N.J. Petch, J. Iron Steel Inst. 174 (1953) 25–28.
[40] C. Wang, C. Wang, J. Xu, P. Zhang, D. Shan, B. Guo, Mater. Sci. Eng. A 636 (2015) 352–360.
[41] C. Keller, E. Hug, X. Feaugas, Int. J. Plast. 27 (2011) 635–654.
[42] X.X. Chen, A.H.W. Ngan, Scr. Mater. 64 (2011) 717–720.
[43] A. Misra, J.P. Hirth, R.G. Hoagland, Acta Mater. 53 (2005) 4817–4824.
[44] J.Y. Zhang, G. Liu, J. Sun, Acta Mater. 61 (2013) 6868–6881.
[45] W. Guo, E. Jägle, J. Yao, V. Maier, S. Korte-Kerzel, J.M. Schneider, D. Raabe, Acta Mater. 80 (2014) 94–106.
[46] I. Knorr, N.M. Cordero, E.T. Lilleodden, C.A. Volkert, Acta Mater. 61 (2013) 4984–4995.
[47] L. Nicola, Y. Xiang, J.J. Vlassak, E. Van der Giessen, A. Needleman, J. Mech. Phys. Solids 54 (2006) 2089–2110.
[48] A.J. Bushby, D.J. Dunstan, Philos. Mag. 91 (2011) 1037–1049.
[49] D. Dunstan, B. Ehrler, R. Bossis, S. Joly, K.M.Y. P'ng, A. Bushby, Phys. Rev. Lett. 103 (2009) 155501.
[50] C. Kirchlechner, J. Keckes, C. Motz, W. Grosinger, M.W. Kapp, J.S. Micha, O. Ulrich, G. Dehm, Acta Mater. 59 (2011) 5618–5626.
[51] C. Niederberger, W.M. Mook, X. Maeder, J. Michler, Mater. Sci. Eng. A 527 (2010) 4306–4311.
[52] R. Maaß, S. Van Petegem, D. Grolimund, H. Van Swygenhoven, D. Kiener, G. Dehm, Appl. Phys. Lett. 92 (2008) 071905.
[53] F. Mompiou, M. Legros, Scr. Mater. 99 (2015) 5–8.
[54] D.S. Gianola, S. Van Petegem, M. Legros, S. Brandstetter, H. Van Swygenhoven, K.J. Hemker, Acta Mater. 54 (2006) 2253–2263.
[55] D. Jang, J.R. Greer, Scr. Mater. 64 (2011) 77–80.
[56] A. Rinaldi, P. Peralta, C. Friesen, K. Sieradzki, Acta Mater. 56 (2008) 511–517.
[57] S. Schreijäg, D. Kaufmann, M. Wenk, O. Kraft, R. Mönig, Acta Mater. 97 (2015) 94–104.
[58] B. Joni, E. Schafler, M. Zehetbauer, G. Tichy, T. Ungar, Acta Mater. 61 (2013) 632–642.
[59] Y. Miyajima, S. Okubo, H. Abe, H. Okumura, T. Fujii, S. Onaka, M. Kato, Mater. Charact. 104 (2015) 101–106.
[60] M. Henning, H. Vehoff, Mater. Sci. Eng. A 452 (2007) 453–602.
[61] J.A. El-Awady, Nat. Commun. 6 (5926) (2015) 1–9.